

Search for a doubly-charged DDK bound state in $\Upsilon(1S, 2S)$ inclusive decays and via direct production in e^+e^- collisions at $\sqrt{s} = 10.520, 10.580, \text{ and } 10.867 \text{ GeV}$

Y. Li,² S. Jia,¹² C. P. Shen,¹² I. Adachi,^{19,15} H. Aihara,⁹⁰ S. Al Said,^{84,40} D. M. Asner,⁴ T. Aushev,²¹ R. Ayad,⁸⁴ V. Babu,⁹ S. Bahinipati,²⁵ P. Behera,²⁸ K. Belous,³² J. Bennett,⁵⁶ M. Bessner,¹⁸ V. Bhardwaj,²⁴ B. Bhuyan,²⁶ T. Bilka,⁶ J. Biswal,³⁶ G. Bonvicini,⁹⁵ A. Bozek,⁶⁵ M. Bračko,^{53,36} T. E. Browder,¹⁸ M. Campajola,^{33,60} D. Červenkov,⁶ M.-C. Chang,¹¹ P. Chang,⁶⁴ A. Chen,⁶² B. G. Cheon,¹⁷ K. Chilikin,⁴⁷ K. Cho,⁴² S.-J. Cho,⁹⁷ S.-K. Choi,¹⁶ Y. Choi,⁸² S. Choudhury,²⁷ D. Cinabro,⁹⁵ S. Cunliffe,⁹ S. Das,⁵² N. Dash,²⁸ G. De Nardo,^{33,60} F. Di Capua,^{33,60} J. Dingfelder,³ Z. Doležal,⁶ T. V. Dong,¹² S. Eidelman,^{5,68,47} D. Epifanov,^{5,68} T. Ferber,⁹ B. G. Fulsom,⁷⁰ R. Garg,⁷¹ V. Gaur,⁹⁴ A. Garmash,^{5,68} A. Giri,²⁷ P. Goldenzweig,³⁷ Y. Guan,⁸ C. Hadjivasiliou,⁷⁰ O. Hartbrich,¹⁸ K. Hayasaka,⁶⁷ H. Hayashii,⁶¹ M. T. Hedges,¹⁸ W.-S. Hou,⁶⁴ C.-L. Hsu,⁸³ K. Inami,⁵⁹ G. Inguglia,³¹ A. Ishikawa,^{19,15} R. Itoh,^{19,15} M. Iwasaki,⁶⁹ Y. Iwasaki,¹⁹ W. W. Jacobs,²⁹ H. B. Jeon,⁴⁵ Y. Jin,⁹⁰ C. W. Joo,³⁸ K. K. Joo,⁷ A. B. Kaliyar,⁸⁵ K. H. Kang,⁴⁵ G. Karyan,⁹ T. Kawasaki,⁴¹ C. Kiesling,⁵⁴ D. Y. Kim,⁸¹ K.-H. Kim,⁹⁷ S. H. Kim,⁷⁸ Y.-K. Kim,⁹⁷ K. Kinoshita,⁸ P. Kodyš,⁶ T. Konno,⁴¹ S. Korpar,^{53,36} D. Kotchetkov,¹⁸ P. Krizan,^{49,36} R. Kroeger,⁵⁶ P. Krokovny,^{5,68} T. Kuhr,⁵⁰ R. Kulasiri,³⁹ M. Kumar,⁵² R. Kumar,⁷⁴ K. Kumara,⁹⁵ Y.-J. Kwon,⁹⁷ K. Lalwani,⁵² J. S. Lange,¹³ I. S. Lee,¹⁷ S. C. Lee,⁴⁵ C. H. Li,⁴⁸ J. Li,⁴⁵ L. K. Li,⁸ Y. B. Li,⁷² L. Li Gioi,⁵⁴ J. Libby,²⁸ K. Lieret,⁵⁰ Z. Liptak,^{18,*} C. MacQueen,⁵⁵ M. Masuda,^{89,75} T. Matsuda,⁵⁷ D. Matvienko,^{5,68,47} M. Merola,^{33,60} K. Miyabayashi,⁶¹ H. Miyata,⁶⁷ R. Mizuk,^{47,21} G. B. Mohanty,⁸⁵ S. Mohanty,^{85,93} T. Mori,⁵⁹ R. Mussa,³⁴ M. Nakao,^{19,15} Z. Natkaniec,⁶⁵ A. Natochii,¹⁸ L. Nayak,²⁷ M. Nayak,⁸⁷ M. Niyama,⁴⁴ N. K. Nisar,⁴ S. Nishida,^{19,15} H. Ono,^{66,67} Y. Onuki,⁹⁰ P. Oskin,⁴⁷ P. Pakhlov,^{47,58} G. Pakhlova,^{21,47} T. Pang,⁷³ S. Pardi,³³ H. Park,⁴⁵ S.-H. Park,⁹⁷ S. Patra,²⁴ S. Paul,^{86,54} T. K. Pedlar,⁵¹ R. Pestotnik,³⁶ L. E. Piilonen,⁹⁴ T. Podobnik,^{49,36} V. Popov,²¹ E. Prencipe,²² M. T. Prim,³⁷ M. Ritter,⁵⁰ M. Röhrken,⁹ A. Rostomyan,⁹ N. Rout,²⁸ G. Russo,⁶⁰ D. Sahoo,⁸⁵ Y. Sakai,^{19,15} S. Sandilya,²⁷ A. Sangal,⁸ L. Santelj,^{49,36} T. Sanuki,⁸⁸ V. Savinov,⁷³ G. Schnell,^{1,23} J. Schueler,¹⁸ C. Schwanda,³¹ Y. Seino,⁶⁷ K. Senyo,⁹⁶ M. E. Sevier,⁵⁵ M. Shapkin,³² C. Sharma,⁵² J.-G. Shiu,⁶⁴ B. Shwartz,^{5,68} A. Sokolov,³² E. Solovieva,⁴⁷ M. Starič,³⁶ Z. S. Stottler,⁹⁴ M. Sumihama,¹⁴ K. Sumisawa,^{19,15} T. Sumiyoshi,⁹² W. Sutcliffe,³ M. Takizawa,^{79,20,76} U. Tamponi,³⁴ K. Tanida,³⁵ F. Tenchini,⁹ M. Uchida,⁹¹ T. Uglov,^{47,21} Y. Unno,¹⁷ S. Uno,^{19,15} S. E. Vahsen,¹⁸ R. Van Tonder,³ G. Varner,¹⁸ A. Vinokurova,^{5,68} V. Vorobyev,^{5,68,47} C. H. Wang,⁶³ E. Wang,⁷³ M.-Z. Wang,⁶⁴ P. Wang,³⁰ M. Watanabe,⁶⁷ S. Watanuki,⁴⁶ E. Won,⁴³ X. Xu,⁸⁰ B. D. Yabsley,⁸³ W. Yan,⁷⁷ S. B. Yang,⁴³ H. Ye,⁹ J. Yelton,¹⁰ J. H. Yin,⁴³ C. Z. Yuan,³⁰ Z. P. Zhang,⁷⁷ V. Zhilich,^{5,68} V. Zhukova,⁴⁷ and V. Zhulanov,^{5,68}

(The Belle Collaboration)

¹University of the Basque Country UPV/EHU, 48080 Bilbao

²Beihang University, Beijing 100191

³University of Bonn, 53115 Bonn

⁴Brookhaven National Laboratory, Upton, New York 11973

⁵Budker Institute of Nuclear Physics SB RAS, Novosibirsk 630090

⁶Faculty of Mathematics and Physics, Charles University, 121 16 Prague

⁷Chonnam National University, Gwangju 61186

⁸University of Cincinnati, Cincinnati, Ohio 45221

⁹Deutsches Elektronen-Synchrotron, 22607 Hamburg

¹⁰University of Florida, Gainesville, Florida 32611

¹¹Department of Physics, Fu Jen Catholic University, Taipei 24205

¹²Key Laboratory of Nuclear Physics and Ion-beam Application (MOE) and Institute of Modern Physics, Fudan University, Shanghai 200443

¹³Justus-Liebig-Universität Gießen, 35392 Gießen

¹⁴Gifu University, Gifu 501-1193

¹⁵SOKENDAI (The Graduate University for Advanced Studies), Hayama 240-0193

¹⁶Gyeongsang National University, Jinju 52828

- ¹⁷*Department of Physics and Institute of Natural Sciences, Hanyang University, Seoul 04763*
- ¹⁸*University of Hawaii, Honolulu, Hawaii 96822*
- ¹⁹*High Energy Accelerator Research Organization (KEK), Tsukuba 305-0801*
- ²⁰*J-PARC Branch, KEK Theory Center, High Energy Accelerator Research Organization (KEK), Tsukuba 305-0801*
- ²¹*Higher School of Economics (HSE), Moscow 101000*
- ²²*Forschungszentrum Jülich, 52425 Jülich*
- ²³*IKERBASQUE, Basque Foundation for Science, 48013 Bilbao*
- ²⁴*Indian Institute of Science Education and Research Mohali, SAS Nagar, 140306*
- ²⁵*Indian Institute of Technology Bhubaneswar, Satya Nagar 751007*
- ²⁶*Indian Institute of Technology Guwahati, Assam 781039*
- ²⁷*Indian Institute of Technology Hyderabad, Telangana 502285*
- ²⁸*Indian Institute of Technology Madras, Chennai 600036*
- ²⁹*Indiana University, Bloomington, Indiana 47408*
- ³⁰*Institute of High Energy Physics, Chinese Academy of Sciences, Beijing 100049*
- ³¹*Institute of High Energy Physics, Vienna 1050*
- ³²*Institute for High Energy Physics, Protvino 142281*
- ³³*INFN - Sezione di Napoli, 80126 Napoli*
- ³⁴*INFN - Sezione di Torino, 10125 Torino*
- ³⁵*Advanced Science Research Center, Japan Atomic Energy Agency, Naka 319-1195*
- ³⁶*J. Stefan Institute, 1000 Ljubljana*
- ³⁷*Institut für Experimentelle Teilchenphysik, Karlsruher Institut für Technologie, 76131 Karlsruhe*
- ³⁸*Kavli Institute for the Physics and Mathematics of the Universe (WPI), University of Tokyo, Kashiwa 277-8583*
- ³⁹*Kennesaw State University, Kennesaw, Georgia 30144*
- ⁴⁰*Department of Physics, Faculty of Science, King Abdulaziz University, Jeddah 21589*
- ⁴¹*Kitasato University, Sagami-hara 252-0373*
- ⁴²*Korea Institute of Science and Technology Information, Daejeon 34141*
- ⁴³*Korea University, Seoul 02841*
- ⁴⁴*Kyoto Sangyo University, Kyoto 603-8555*
- ⁴⁵*Kyungpook National University, Daegu 41566*
- ⁴⁶*Université Paris-Saclay, CNRS/IN2P3, IJCLab, 91405 Orsay*
- ⁴⁷*P.N. Lebedev Physical Institute of the Russian Academy of Sciences, Moscow 119991*
- ⁴⁸*Liaoning Normal University, Dalian 116029*
- ⁴⁹*Faculty of Mathematics and Physics, University of Ljubljana, 1000 Ljubljana*
- ⁵⁰*Ludwig Maximilians University, 80539 Munich*
- ⁵¹*Luther College, Decorah, Iowa 52101*
- ⁵²*Malaviya National Institute of Technology Jaipur, Jaipur 302017*
- ⁵³*University of Maribor, 2000 Maribor*
- ⁵⁴*Max-Planck-Institut für Physik, 80805 München*
- ⁵⁵*School of Physics, University of Melbourne, Victoria 3010*
- ⁵⁶*University of Mississippi, University, Mississippi 38677*
- ⁵⁷*University of Miyazaki, Miyazaki 889-2192*
- ⁵⁸*Moscow Physical Engineering Institute, Moscow 115409*
- ⁵⁹*Graduate School of Science, Nagoya University, Nagoya 464-8602*
- ⁶⁰*Università di Napoli Federico II, 80126 Napoli*

- ⁶¹*Nara Women's University, Nara 630-8506*
- ⁶²*National Central University, Chung-li 32054*
- ⁶³*National United University, Miao Li 36003*
- ⁶⁴*Department of Physics, National Taiwan University, Taipei 10617*
- ⁶⁵*H. Niewodniczanski Institute of Nuclear Physics, Krakow 31-342*
- ⁶⁶*Nippon Dental University, Niigata 951-8580*
- ⁶⁷*Niigata University, Niigata 950-2181*
- ⁶⁸*Novosibirsk State University, Novosibirsk 630090*
- ⁶⁹*Osaka City University, Osaka 558-8585*
- ⁷⁰*Pacific Northwest National Laboratory, Richland, Washington 99352*
- ⁷¹*Panjab University, Chandigarh 160014*
- ⁷²*Peking University, Beijing 100871*
- ⁷³*University of Pittsburgh, Pittsburgh, Pennsylvania 15260*
- ⁷⁴*Punjab Agricultural University, Ludhiana 141004*
- ⁷⁵*Research Center for Nuclear Physics, Osaka University, Osaka 567-0047*
- ⁷⁶*Meson Science Laboratory, Cluster for Pioneering Research, RIKEN, Saitama 351-0198*
- ⁷⁷*Department of Modern Physics and State Key Laboratory of Particle Detection and Electronics, University of Science and Technology of China, Hefei 230026*
- ⁷⁸*Seoul National University, Seoul 08826*
- ⁷⁹*Showa Pharmaceutical University, Tokyo 194-8543*
- ⁸⁰*Soochow University, Suzhou 215006*
- ⁸¹*Soongsil University, Seoul 06978*
- ⁸²*Sungkyunkwan University, Suwon 16419*
- ⁸³*School of Physics, University of Sydney, New South Wales 2006*
- ⁸⁴*Department of Physics, Faculty of Science, University of Tabuk, Tabuk 71451*
- ⁸⁵*Tata Institute of Fundamental Research, Mumbai 400005*
- ⁸⁶*Department of Physics, Technische Universität München, 85748 Garching*
- ⁸⁷*School of Physics and Astronomy, Tel Aviv University, Tel Aviv 69978*
- ⁸⁸*Department of Physics, Tohoku University, Sendai 980-8578*
- ⁸⁹*Earthquake Research Institute, University of Tokyo, Tokyo 113-0032*
- ⁹⁰*Department of Physics, University of Tokyo, Tokyo 113-0033*
- ⁹¹*Tokyo Institute of Technology, Tokyo 152-8550*
- ⁹²*Tokyo Metropolitan University, Tokyo 192-0397*
- ⁹³*Utkal University, Bhubaneswar 751004*
- ⁹⁴*Virginia Polytechnic Institute and State University, Blacksburg, Virginia 24061*
- ⁹⁵*Wayne State University, Detroit, Michigan 48202*
- ⁹⁶*Yamagata University, Yamagata 990-8560*
- ⁹⁷*Yonsei University, Seoul 03722*

We report the results of a first search for a doubly-charged DDK bound state, denoted the R^{++} , in $\Upsilon(1S)$ and $\Upsilon(2S)$ inclusive decays and via direct production in e^+e^- collisions at $\sqrt{s} = 10.520$, 10.580 , and 10.867 GeV. The search uses data accumulated with the Belle detector at the KEKB asymmetric-energy e^+e^- collider. No significant signals are observed in the $D^+D_s^{*+}$ invariant-mass spectra of all studied modes. The 90% credibility level upper limits on their product branching fractions in $\Upsilon(1S)$ and $\Upsilon(2S)$ inclusive decays ($\mathcal{B}(\Upsilon(1S,2S) \rightarrow R^{++} + \text{anything}) \times \mathcal{B}(R^{++} \rightarrow D^+D_s^{*+})$), and the product values of Born cross section and branching fraction in e^+e^- collisions ($\sigma(e^+e^- \rightarrow R^{++} + \text{anything}) \times \mathcal{B}(R^{++} \rightarrow D^+D_s^{*+})$) at $\sqrt{s} = 10.520$, 10.580 , and 10.867 GeV under

different assumptions of R^{++} masses varying from 4.13 to 4.17 GeV/ c^2 , and widths varying from 0 to 5 MeV are obtained.

I. INTRODUCTION

In 2003, a narrow resonance near 2.32 GeV/ c^2 , the $D_{s0}^*(2317)^+$, was observed by BaBar [1] via its decay to $D_s^+\pi^0$. The $D_{s0}^*(2317)^+$ was subsequently confirmed by CLEO [2] and Belle [3]. The observed low mass and narrow width of the $D_{s0}^*(2317)^+$ strongly disfavor the interpretation of this state as a P -wave $c\bar{s}$ state, both in potential model [4–9] and lattice Quantum Chromodynamics (QCD) [10, 11] descriptions. Inclusion of charge-conjugate decays is implicitly assumed throughout this analysis. Instead, it has been proposed as a possible candidate for a DK molecule [12–17], a $(cq)(\bar{s}\bar{q})$ tetraquark state [18–20], or a mixture of a $c\bar{s}$ state and tetraquark [21–28]. The absolute branching fraction of $D_{s0}^*(2317)^+ \rightarrow D_s^+\pi^0$ was measured by BESIII to be $1.00^{+0.00}_{-0.14} \pm 0.14$ [29]. This result indicates that the $D_{s0}^*(2317)^+$ has a much smaller branching fraction to $D_s^{*+}\gamma$ than to $D_s^+\pi^0$, and this agrees with the expectation of the conventional $c\bar{s}$ state hypothesis [30] or the hadronic molecule picture of DK [31, 32]. There have been theoretical interpretations of the $D_{s0}^*(2317)^+$ and $D_{s1}(2460)^+$ as chiral partners, with production mechanisms related to the spontaneous breaking of chiral symmetry [33, 34].

By exchanging a kaon, a $D^+D_{s0}^*(2317)^+$ molecular state can be formed with a binding energy of 5 – 15 MeV, regardless of whether the $D_{s0}^*(2317)^+$ is treated as a $c\bar{s}$ state or a DK molecule [35]. In Ref. [36], the authors studied the DDK system in a coupled-channel approach, where an isospin 1/2 state, denoted the R^{++} , is formed at 4140 MeV/ c^2 when the $D_{s0}^*(2317)^+$ is generated from the DK subsystem. The R^{++} can be interpreted as a $D^+D_{s0}^*(2317)^+$ molecule-like state with exotic properties: doubly-charged and doubly-charmed. Hereinafter we also refer to this predicted state as R^{++} .

An R^{++} with the properties described above would be able to decay via $R^{++} \rightarrow D^+D_{s0}^*(2317)^+$, where $D_{s0}^*(2317)^+ \rightarrow D_s^+\pi^0$ is an isospin-violating process. The alternative processes are via triangle diagrams into $R^{++} \rightarrow D^+D_s^{*+}$ and $R^{++} \rightarrow D_s^+D^{*+}$ [36–38]. The mass of R^{++} is predicted to be in the range of 4.13 to 4.17 GeV/ c^2 [38]. The predicted partial decay width of $R^{++} \rightarrow D^+D_s^{*+}$ is much larger than that of $R^{++} \rightarrow D_s^+D^{*+}$; they are $\Gamma(R^{++} \rightarrow D^+D_s^{*+}) = (2.30 - 2.49)$ MeV and $\Gamma(R^{++} \rightarrow D_s^+D^{*+}) = (0.26 - 0.29)$ MeV [38], respectively.

The question whether $QQ\bar{q}\bar{q}$ tetraquarks with two heavy quarks Q and two light antiquarks \bar{q} are stable

or unstable against decay into two $Q\bar{q}$ mesons has a long history. It has been largely undecided, mainly due to a lack of experimental information about the strength of the interaction between two heavy quarks. The discovery of the doubly-charmed baryon Ξ_{cc}^{++} by LHCb [39] has provided the crucial experimental input [40, 41]. In Ref. [41], the authors predicted the existence of novel narrow doubly-heavy tetraquark states of the form $QQ\bar{q}\bar{q}$ with the method based on the heavy-quark symmetry, and found that a doubly-charmed tetraquark with a mass of 4156 MeV/ c^2 and a J^P of 1^+ decaying into a final state of $D^+D_s^{*+}$ can be formed. Thus the $D^+D_s^{*+}$ final state is a good channel to search for such a tetraquark state.

In this paper, we search for a doubly-charged DDK bound state in the $D^+D_s^{*+}$ final state in $\Upsilon(1S)$ and $\Upsilon(2S)$ inclusive decays, and via direct production in e^+e^- collisions at $\sqrt{s} = 10.520, 10.580$, and 10.867 GeV. We report a search for the R^{++} with masses varying from 4.13 to 4.17 GeV/ c^2 and widths varying from 0 to 5 MeV.

II. THE DATA SAMPLE AND THE BELLE DETECTOR

This analysis utilizes (5.74 ± 0.09) fb $^{-1}$ of data collected at the $\Upsilon(1S)$ peak $[(102 \pm 3)$ million $\Upsilon(1S)$ events], (24.91 ± 0.35) fb $^{-1}$ of data collected at the $\Upsilon(2S)$ peak $[(158 \pm 4)$ million $\Upsilon(2S)$ events], a data sample of (89.5 ± 1.3) fb $^{-1}$ collected at $\sqrt{s} = 10.520$ GeV, a data sample of (711.0 ± 10.0) fb $^{-1}$ collected at $\sqrt{s} = 10.580$ GeV [$\Upsilon(4S)$ peak], and a data sample of (121.4 ± 1.7) fb $^{-1}$ collected at $\sqrt{s} = 10.867$ GeV [$\Upsilon(5S)$ peak]. All the data were collected with the Belle detector [42] operating at the KEKB asymmetric-energy e^+e^- collider [43]. The Belle detector is described in detail in Ref. [42]. It is a large-solid-angle magnetic spectrometer consisting of a silicon vertex detector, a 50-layer central drift chamber (CDC), an array of aerogel threshold Cherenkov counters (ACC), a barrel-like arrangement of time-of-flight scintillation counters (TOF), and an electromagnetic calorimeter comprising CsI(Tl) crystals (ECL) located inside a superconducting solenoid coil that provides a 1.5 T magnetic field. An iron flux return comprising resistive plate chambers (RPCs) placed outside the coil is instrumented to detect K_L^0 mesons and to identify muons (KLM).

Monte Carlo (MC) signal samples are generated with EVTGEN [44] to determine signal shapes and efficiencies. Initial-state radiation (ISR) is taken into account by assuming that the cross sections follow a $1/s$ dependence in $e^+e^- \rightarrow R^{++} + \text{anything}$ reactions, where s is the center-of-mass energy squared. The mass of R^{++} is chosen from 4.13 to 4.17 GeV/ c^2 in steps of 2.5 MeV/ c^2 ,

*now at University of Hiroshima

with a width varying from 0 to 5 MeV in steps of 1 MeV. These events are processed by a detector simulation based on GEANT3 [45].

Inclusive MC samples of $\Upsilon(1S, 2S)$ decays, $\Upsilon(4S) \rightarrow B^+B^-/B^0\bar{B}^0$, $\Upsilon(5S) \rightarrow B_s^{(*)}\bar{B}_s^{(*)}$, and $e^+e^- \rightarrow q\bar{q}$ ($q = u, d, s, c$) at $\sqrt{s} = 10.520, 10.580$, and 10.867 GeV corresponding to four times the integrated luminosity of data are used to study possible peaking backgrounds.

III. COMMON EVENT SELECTION CRITERIA

For well-reconstructed charged tracks, except those from $K_S^0 \rightarrow \pi^+\pi^-$ decays, the impact parameters perpendicular to and along the beam direction with respect to the nominal interaction point (IP) are required to be less than 0.5 cm and 2 cm, respectively, and the transverse momentum in the laboratory frame is required to be larger than 0.1 GeV/c. For the particle identification (PID) of a well-reconstructed charged track, information from different detector subsystems, including specific ionization in the CDC, time measurement in the TOF, and the response of the ACC, is combined to form a likelihood \mathcal{L}_i [46] for particle species i , where $i = \pi$ or K . Tracks with $R_K = \mathcal{L}_K/(\mathcal{L}_K + \mathcal{L}_\pi) < 0.4$ are identified as pions with an efficiency of 96%, while 5% of kaons are misidentified as pions; tracks with $R_K > 0.6$ are identified as kaons with an efficiency of 95%, while 4% of pions are misidentified as kaons. Except for tracks from K_S^0 decays, all charged tracks are required to be positively identified by the above procedures.

An ECL cluster is taken as a photon candidate if it does not match the extrapolation of any charged track. The energy of the photon is required to be greater than 50 MeV.

The K_S^0 candidates are first reconstructed from pairs of oppositely charged tracks, which are treated as pions, with a production vertex significantly separated from the average IP, then selected using an artificial neural network [47] based on two sets of input variables [48]. The ϕ and $\bar{K}^*(892)^0$ candidates are reconstructed using K^+K^- and $K^-\pi^+$ decay modes, respectively. The invariant masses of the K_S^0 and ϕ candidates are required to be within 7 MeV/ c^2 of the corresponding nominal masses ($> 90\%$ signal events are retained).

We reconstruct D^+ mesons in the $K^-\pi^+\pi^+$ and $K_S^0(\rightarrow \pi^+\pi^-)\pi^+$ decay channels, and D_s^+ mesons in the $\phi\pi^+$ and $\bar{K}^*(892)^0K^+$ decay channels. We perform vertex- and mass-constrained fits for D^+ and D_s^+ candidates, and require $\chi_{\text{vertex}}^2/n.d.f. < 20$ ($> 97\%$ selection efficiency according to MC simulation). The selected D_s^+ candidate is combined with a photon to form a D_s^{*+} candidate, and a mass-constrained fit is performed to improve its momentum resolution.

The signal mass windows for $\bar{K}^*(892)^0$, D^+ , D_s^+ , and D_s^{*+} candidates have been optimized by maximizing the Punzi parameter $S/(3/2 + \sqrt{B})$ [49]. Here, S is the number of R^{++} signal events in the MC-simulated $\Upsilon(2S) \rightarrow R^{++} + \text{anything}$ sample with the mass and width of R^{++} fixed at 4.13 GeV/ c^2 and 2 MeV assuming $\mathcal{B}(\Upsilon(2S) \rightarrow R^{++} + \text{anything}) \times \mathcal{B}(R^{++} \rightarrow D^+D_s^{*+}) = 10^{-4}$, and B is the number of background events in the R^{++} signal window. The number of background events is obtained from the normalized M_{D^+} and $M_{D_s^{*+}}$ sidebands in the data requiring $4.12 \text{ GeV}/c^2 \leq M_{D^+} \leq 4.14 \text{ GeV}/c^2$ as the R^{++} signal region (about 3σ according to signal MC simulations). The optimized signal regions are $|M_{K^-\pi^+} - m_{\bar{K}^*(892)^0}| < 60 \text{ MeV}/c^2$, $|M_{K^-\pi^+\pi^+}/K_S^0\pi^+ - m_{D^+}| < 6 \text{ MeV}/c^2$, $|M_{\phi\pi^+/\bar{K}^*(892)^0K^+} - m_{D_s^+}| < 6 \text{ MeV}/c^2$, and $|M_{\gamma D_s^+} - m_{D_s^{*+}}| < 9 \text{ MeV}/c^2$ for $\bar{K}^*(892)^0$, D^+ , D_s^+ , and D_s^{*+} candidates ($> 80\%$ signal events are retained for each intermediate state), respectively, where $m_{\bar{K}^*(892)^0}$, $m_{D_s^+}$, m_{D^+} , and $m_{D_s^{*+}}$ are the nominal masses of $\bar{K}^*(892)^0$, D_s^+ , D^+ , and D_s^{*+} mesons [50]. For the process $\Upsilon(1S) \rightarrow R^{++} + \text{anything}$ and $e^+e^- \rightarrow R^{++} + \text{anything}$ at $\sqrt{s} = 10.520, 10.580$, and 10.867 GeV, the optimized signal regions of intermediate states are the same.

Finally, when the D^+ and D_s^{*+} candidates are combined to form R^{++} candidates, all the combinations are preserved for further analysis. The fraction of events where multiple combinations are selected as R^{++} candidates is 14% in data, which is consistent with the MC simulation.

IV. $\Upsilon(1S, 2S) \rightarrow R^{++} + \text{ANYTHING}$

In this section, we search for the doubly-charged DDK bound state in $\Upsilon(1S)$ and $\Upsilon(2S)$ inclusive decays. After applying the aforementioned common event selections, the invariant-mass distributions of the D_s^+ , D^+ , and D_s^{*+} candidates from the $\Upsilon(1S)$ and $\Upsilon(2S)$ data samples are shown in Figs. 1 and 2, respectively, together with results of the fits described below. When drawing each distribution, the signal mass windows of other intermediate states are required. No clear D_s^+ , D^+ , and D_s^{*+} signals are observed. In the fits, the D_s^+ and D^+ signal shapes are described by double-Gaussian functions, and the D_s^{*+} signal shape is described by a Novosibirsk function [51], where the values of parameters are fixed to those obtained from the fits to the corresponding signal MC distributions. The backgrounds are parametrized by first-order polynomial functions for D_s^+ and D^+ , and a second-order polynomial function for D_s^{*+} .

Figure 3 shows the scatter plots of $M_{D_s^{*+}}$ versus M_{D^+} from $\Upsilon(1S)$ and $\Upsilon(2S)$ data samples, respectively. The central solid boxes show the signal regions of D^+ and

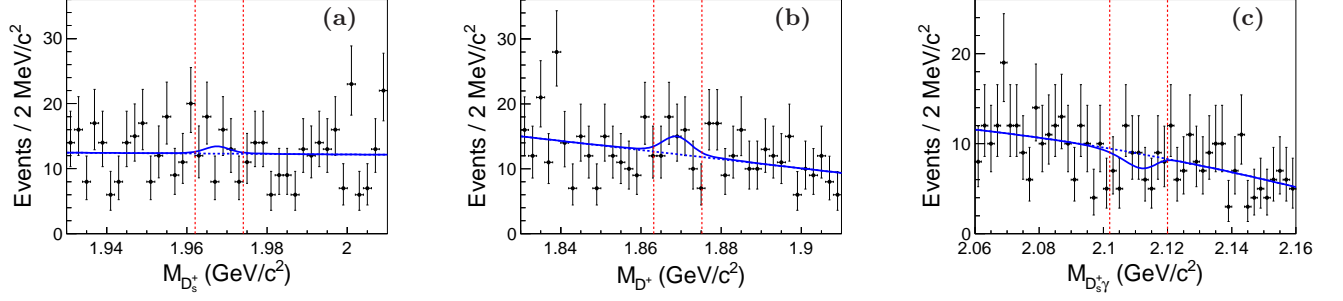


FIG. 1: The invariant-mass spectra of the (a) D_s^+ , (b) D^+ , and (c) D_s^{*+} candidates summed over four reconstructed modes from $\Upsilon(1S)$ data. The points with error bars represent the data, the solid curves show the results of the best fits to the data, and the blue dashed curves are the fitted backgrounds. The red dashed lines show the required signal regions.

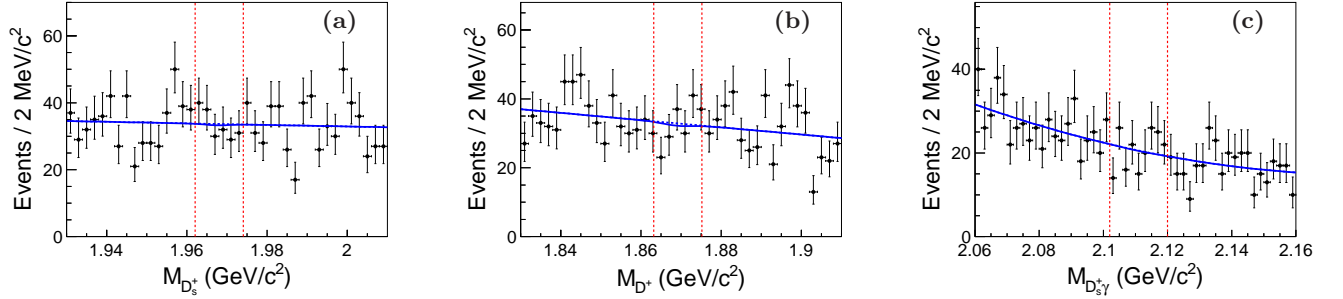


FIG. 2: The invariant-mass spectra of the (a) D_s^+ , (b) D^+ , and (c) D_s^{*+} candidates summed over four reconstructed modes from $\Upsilon(2S)$ data. The points with error bars represent the data, the solid curves show the results of the best fits to the data, and the blue dashed curves are the fitted backgrounds. The red dashed lines show the required signal regions.

D_s^{*+} . To check possible peaking backgrounds, the M_{D^+} and $M_{D_s^{*+}}$ sidebands are selected, represented by the blue dashed (the total number of sideband events is denoted as N_1) and red dash-dotted boxes (the total number of sideband events is denoted as N_2) in Fig. 3. The background contribution from the normalized M_{D^+} and $M_{D_s^{*+}}$ sidebands is estimated to be $0.5 \times N_1 - 0.25 \times N_2$.

Figure 4 shows the invariant-mass distributions of $D^+D_s^{*+}$ in the $\Upsilon(1S)$ and $\Upsilon(2S)$ data samples, together with the backgrounds from the normalized M_{D^+} and $M_{D_s^{*+}}$ sidebands. There are no evident signals for R^{++} states at the expected masses. An unbinned extended maximum-likelihood fit repeated with $M_{R^{++}}$ from 4.13 to 4.17 GeV/c^2 in steps of 2.5 MeV/c^2 , and $\Gamma_{R^{++}}$ from 0 to 5 MeV in steps of 1 MeV is performed to the $M_{D^+D_s^{*+}}$ distribution. The signal shapes of R^{++} are described by a Gaussian function ($\Gamma_{R^{++}} = 0$) or Breit-Wigner (BW) functions convolved with Gaussian functions ($\Gamma_{R^{++}} \neq 0$), where the parameters are fixed to those obtained from the fits to the corresponding MC simulated distributions. The mass resolution of the $M_{D^+D_s^{*+}}$ is $(1.7 \pm 0.1) \text{ MeV}/c^2$. There are no peaking backgrounds found in the M_{D^+} and $M_{D_s^{*+}}$ sidebands or in the $\Upsilon(1S, 2S)$ inclusive MC samples [52], so first-order polynomial functions with free parameters are taken as

background shapes. The fitted results with the R^{++} mass fixed at 4.14 GeV/c^2 and width fixed at 2 MeV are shown in Fig. 4 as an example. Assuming a Gaussian shape of the likelihoods, the local R^{++} significance is calculated using $\sqrt{-2 \ln(\mathcal{L}_0/\mathcal{L}_{\max})}$, where \mathcal{L}_0 and \mathcal{L}_{\max} are the likelihoods of the fits without and with a signal component, respectively. The fitted R^{++} signal yields at typically assumed mass points with $\Gamma_{R^{++}}$ fixed at values ranging from 0 to 5 MeV in steps of 1 MeV and the corresponding statistical significances are listed in Table I.

The branching fraction, $\mathcal{B}(\Upsilon(1S, 2S) \rightarrow R^{++} + \text{anything}) \times \mathcal{B}(R^{++} \rightarrow D^+D_s^{*+})$, is calculated using

$$\frac{N^{\text{fit}}}{N_{\Upsilon(1S, 2S)} \times \sum_i \varepsilon_i \mathcal{B}_i},$$

where N^{fit} is the fitted number of signal events, $N_{\Upsilon(1S)} = 1.02 \times 10^8$ and $N_{\Upsilon(2S)} = 1.58 \times 10^8$ are the total numbers of $\Upsilon(1S)$ and $\Upsilon(2S)$ events, the index i runs for all final-state modes with ε_i being the corresponding efficiency and \mathcal{B}_i the product of all secondary branching fractions of the mode i [$\mathcal{B}_1 = \mathcal{B}(D^+ \rightarrow K^+\pi^+\pi^+)\mathcal{B}(D_s^{*+} \rightarrow D_s^+\gamma)\mathcal{B}(D_s^+ \rightarrow \phi(\rightarrow K^+K^-)\pi^+)$, $\mathcal{B}_2 = \mathcal{B}(D^+ \rightarrow K_S^0\pi^+)\mathcal{B}(K_S^0 \rightarrow \pi^+\pi^-)\mathcal{B}(D_s^{*+} \rightarrow D_s^+\gamma)\mathcal{B}(D_s^+ \rightarrow \phi(\rightarrow$

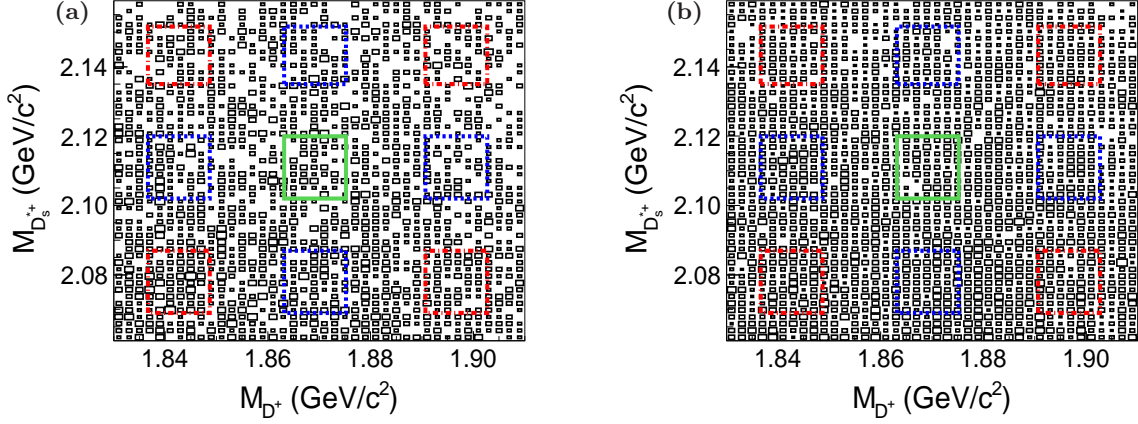


FIG. 3: The scatter plots of $M_{D_s^{*+}}$ versus M_{D^+} from (a) $\Upsilon(1S)$ and (b) $\Upsilon(2S)$ data samples. The central solid boxes define the signal regions, and the red dash-dotted and blue dashed boxes show the M_{D^+} and $M_{D_s^{*+}}$ sideband regions described in the text.

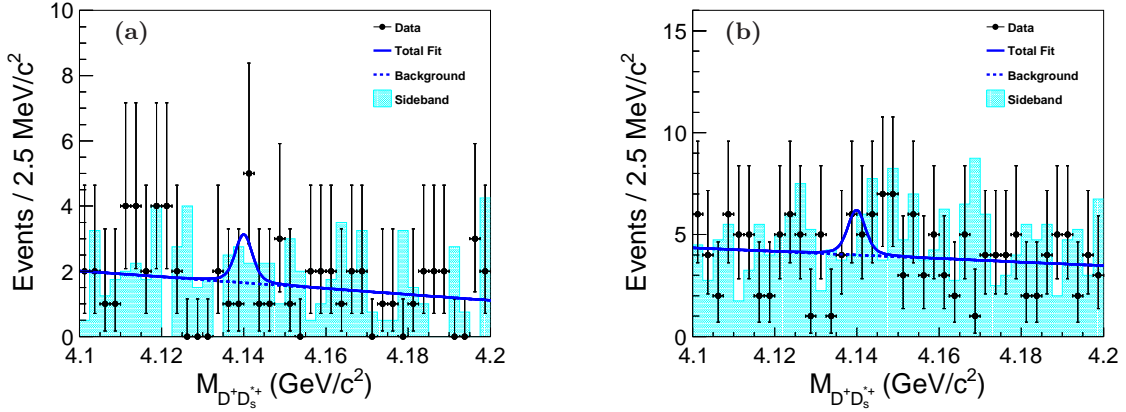


FIG. 4: The invariant-mass spectra of $D^+ D_s^{*+}$ in the (a) $\Upsilon(1S)$ and (b) $\Upsilon(2S)$ data samples. The cyan shaded histograms are from the normalized M_{D^+} and $M_{D_s^{*+}}$ sideband events. The blue solid curves show the fitted results with the R^{++} mass fixed at 4.14 GeV/c^2 and width fixed at 2 MeV, and the blue dashed curves are the fitted backgrounds.

$K^+ K^- \pi^+$), $\mathcal{B}_3 = \mathcal{B}(D^+ \rightarrow K^- \pi^+ \pi^+) \mathcal{B}(D_s^{*+} \rightarrow D_s^+ \gamma) \mathcal{B}(D_s^+ \rightarrow \bar{K}^*(892)^0 (\rightarrow K^- \pi^+) K^+)$, $\mathcal{B}_4 = \mathcal{B}(D^+ \rightarrow K_S^0 \pi^+) \mathcal{B}(K_S^0 \rightarrow \pi^+ \pi^-) \mathcal{B}(D_s^{*+} \rightarrow D_s^+ \gamma) \mathcal{B}(D_s^+ \rightarrow \bar{K}^*(892)^0 (\rightarrow K^- \pi^+) K^+)$. The calculated values of $\mathcal{B}(\Upsilon(1S, 2S) \rightarrow R^{++} + \text{anything}) \times \mathcal{B}(R^{++} \rightarrow D^+ D_s^{*+})$ at typically assumed mass points are listed in Table I.

Since the statistical significance in each case is less than 3σ , Bayesian upper limits at the 90% credibility level (C.L.) on the numbers of signal events (N^{UL}) assuming it follows a Poisson distribution with a uniform prior probability density function are determined by solving the equation $\int_0^{N^{\text{UL}}} \mathcal{L}(x) dx / \int_0^{+\infty} \mathcal{L}(x) dx = 0.9$, where x is the number of fitted signal events and $\mathcal{L}(x)$ is the likelihood function in the fit to data. Taking into account the systematic uncertainties discussed below, the likelihood curve is convolved with a Gaussian

function whose width equals the corresponding total multiplicative systematic uncertainty. The calculated 90% C.L. upper limits on the numbers of signal events and the product branching fractions ($\mathcal{B}^{\text{UL}}(\Upsilon(1S, 2S) \rightarrow R^{++} + \text{anything}) \times \mathcal{B}(R^{++} \rightarrow D^+ D_s^{*+})$) in $\Upsilon(1S)$ and $\Upsilon(2S)$ inclusive decays at typically assumed mass points with width fixed at values ranging from 0 to 5 MeV are listed in Table I. The 90% C.L. upper limits on the product branching fractions for all hypothetical R^{++} masses with widths varying from 0 to 5 MeV are graphically shown in Fig. 5.

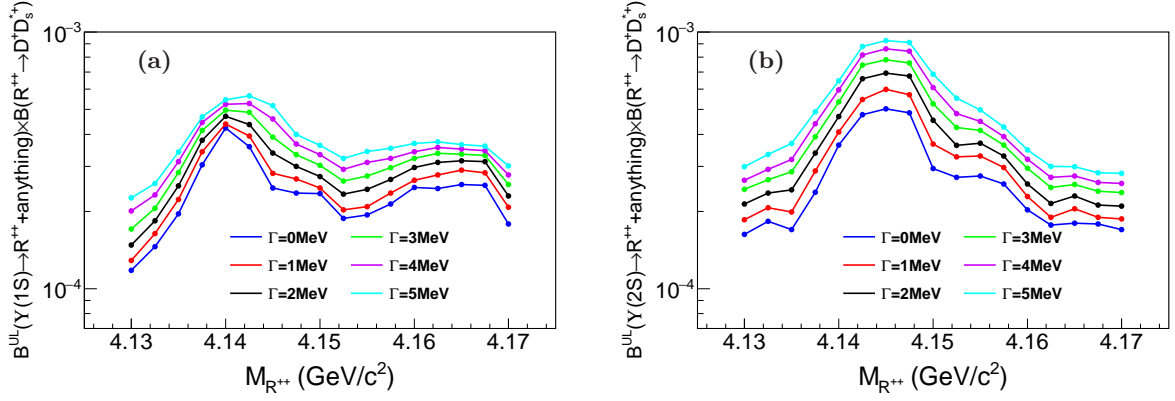


FIG. 5: The 90% C.L. upper limits on (a) $\mathcal{B}(\Upsilon(1S) \rightarrow R^{++} + \text{anything}) \times \mathcal{B}(R^{++} \rightarrow D^+ D_s^{*+})$ and (b) $\mathcal{B}(\Upsilon(2S) \rightarrow R^{++} + \text{anything}) \times \mathcal{B}(R^{++} \rightarrow D^+ D_s^{*+})$ as a function of the assumed R^{++} masses with widths varying from 0 to 5 MeV in steps of 1 MeV.

V. $e^+e^- \rightarrow R^{++} + \text{ANYTHING}$ AT $\sqrt{s} = 10.520, 10.580, \text{ AND } 10.867 \text{ GeV}$

In this section, we search for the doubly-charged DDK bound state via direct production in e^+e^- collisions at $\sqrt{s} = 10.520, 10.580, \text{ and } 10.867 \text{ GeV}$. After the application of the selection criteria, the invariant-mass distributions of D_s^+ , D^+ , and D_s^{*+} candidates from $\sqrt{s} = 10.520, 10.580, \text{ and } 10.867 \text{ GeV}$ data samples are shown in Figs. 6, 7, and 8, respectively, together with results of the fits. When drawing each distribution, the signal mass windows of other intermediate states are required. Since the $\sqrt{s}=10.520 \text{ GeV}$ data sample is below the $B_{(s)}\bar{B}_{(s)}$ threshold, there are no D_s^+ , D^+ , or D_s^{*+} candidates from the $B_{(s)}\bar{B}_{(s)}$ decays, and due to the limited data-set size, no clear D_s^+ , D^+ , or D_s^{*+} signals are observed in this data sample. In the $\sqrt{s} = 10.580$ and 10.867 GeV data samples, evident D_s^+ and D^+ signals, and weak D_s^{*+} signals are seen. In the fits, the D_s^+ and D^+ signal shapes are described by double-Gaussian functions, and the D_s^{*+} signal shape is described by a Novosibirsk function [51], where the values of parameters are fixed to those obtained from fits to corresponding signal MC distributions. The backgrounds are parametrized by first-order polynomial functions for D_s^+ and D^+ , and a second-order polynomial function for D_s^{*+} .

The scatter plots of $M_{D_s^{*+}}$ versus M_{D^+} from the $\sqrt{s} = 10.520, 10.580, \text{ and } 10.867 \text{ GeV}$ data samples are shown in Figs. 9(a), (b), and (c), respectively. The central solid boxes show the D^+ and D_s^{*+} signal regions, and the blue dashed and red dash-dotted boxes show the M_{D^+} and $M_{D_s^{*+}}$ sidebands. The background contribution from the normalized M_{D^+} and $M_{D_s^{*+}}$ sidebands is estimated using the same method as described in Sec. IV.

Figure 10 shows the invariant-mass distributions of

$D^+ D_s^{*+}$ from $\sqrt{s} = 10.520, 10.580, \text{ and } 10.867 \text{ GeV}$ data samples, respectively, together with the backgrounds from the normalized M_{D^+} and $M_{D_s^{*+}}$ sidebands. There are no significant signals for R^{++} states in any of the data samples. An unbinned extended maximum-likelihood fit is performed to the $M_{D^+ D_s^{*+}}$ distribution in a way similar to the methods in Sec. IV. The fitted results with the $M_{R^{++}}$ fixed at $4.14 \text{ GeV}/c^2$ and $\Gamma_{R^{++}}$ fixed at 2 MeV are shown in Fig. 10 as an example. The local R^{++} significance is calculated using the same method as described in Sec. IV. The fitted R^{++} signal yields at typically assumed mass points with $\Gamma_{R^{++}}$ fixed at values ranging from 0 to 5 MeV in steps of 1 MeV and the corresponding statistical significances are listed in Table II.

The product of Born cross section and branching fraction $\sigma(e^+e^- \rightarrow R^{++} + \text{anything}) \times \mathcal{B}(R^{++} \rightarrow D^+ D_s^{*+})$ is calculated from the following formula:

$$\frac{N^{\text{fit}} \times |1 - \prod|^2}{\mathcal{L} \times \sum_i \varepsilon_i \mathcal{B}_i \times (1 + \delta)_{\text{ISR}}},$$

where N^{fit} is the number of fitted signal yields in data, $|1 - \prod|^2$ is the vacuum polarization factor, \mathcal{L} is the integrated luminosity, the index i runs for all final-state modes with ε_i being the corresponding efficiency and \mathcal{B}_i the product of all secondary branching fractions of the mode i , and $(1 + \delta)_{\text{ISR}}$ is the radiative correction factor. The radiative correction factors $(1 + \delta)_{\text{ISR}}$ are 0.710, 0.710, and 0.707 calculated using formulae given in Ref. [53] for $\sqrt{s} = 10.520, 10.580, \text{ and } 10.867 \text{ GeV}$, respectively; the values of $|1 - \prod|^2$ [54] are 0.931, 0.930, and 0.929 for $\sqrt{s} = 10.520, 10.580, \text{ and } 10.867 \text{ GeV}$. In the calculation of $(1 + \delta)_{\text{ISR}}$, we assume that the dependence of the cross section on s is $1/s$. The calculated values of $\sigma(e^+e^- \rightarrow R^{++} + \text{anything}) \times \mathcal{B}(R^{++} \rightarrow D^+ D_s^{*+})$ at $\sqrt{s} = 10.520, 10.580, \text{ and } 10.867 \text{ GeV}$ under typical assumptions of R^{++} mass are

TABLE I: Summary of the 90% C.L. upper limits on the product branching fractions for $\Upsilon(1S, 2S) \rightarrow R^{++} + \text{anything}$ with $R^{++} \rightarrow D^+ D_s^{*+}$ under typical assumptions of R^{++} mass ($M_{R^{++}}$ in GeV/c^2) and width ($\Gamma_{R^{++}}$ in MeV) as examples, where N^{fit} is the number of fitted signal events, N^{UL} is the 90% C.L. upper limit on the number of signal events taking into account systematic uncertainties, $\Sigma(\sigma)$ is the local R^{++} significance, $\Sigma_i(\epsilon_i \mathcal{B}_i)$ is the sum of product of the detection efficiency and the product of all secondary branching fractions for each reconstruction mode, σ_{multi} is the total multiplicative systematic uncertainty, σ_{add} is the additive systematic uncertainty, $\mathcal{B}(\Upsilon(1S, 2S) \rightarrow R^{++} + \text{anything}) \times \mathcal{B}(R^{++} \rightarrow D^+ D_s^{*+})$ is the product branching fraction for $\Upsilon(1S, 2S) \rightarrow R^{++} + \text{anything}$ with $R^{++} \rightarrow D^+ D_s^{*+}$, and $\mathcal{B}^{\text{UL}}(\mathcal{B}^{\text{UL}}(\Upsilon(1S, 2S) \rightarrow R^{++} + \text{anything}) \times \mathcal{B}(R^{++} \rightarrow D^+ D_s^{*+}))$ is the 90% C.L. upper limit on the product branching fraction with systematic uncertainties included.

$M_{R^{++}}$	$\Gamma_{R^{++}}$	N^{fit}	N^{UL}	$\Sigma(\sigma)$	$\Sigma_i(\epsilon_i \mathcal{B}_i) (\times 10^{-5})$	$\sigma_{\text{multi}}(\%)$	$\sigma_{\text{add}}(\%)$	$\mathcal{B}(\times 10^{-5})$	$\mathcal{B}^{\text{UL}}(\times 10^{-5})$
4.13	0	$-4.2 \pm 3.7 / -2.6 \pm 2.7$	2.7 / 5.4	- / -	22.4/21.0	8.0/8.1	3.5 / 5.9	$-18.4 \pm 16.2 / -7.8 \pm 8.1$	11.8/16.3
4.13	1	$-4.0 \pm 3.9 / -3.3 \pm 3.3$	2.9 / 6.1	- / -	22.1/20.8	8.0/8.1	3.8 / 6.2	$-17.7 \pm 17.3 / -10.0 \pm 10.0$	12.9/18.6
4.13	2	$-4.1 \pm 4.3 / -3.9 \pm 3.8$	3.3 / 6.9	- / -	21.9/20.4	8.0/8.1	6.5 / 7.8	$-18.4 \pm 19.2 / -12.1 \pm 11.8$	14.8/21.4
4.13	3	$-4.5 \pm 4.8 / -4.5 \pm 4.3$	3.8 / 7.7	- / -	21.8/20.0	8.0/8.1	11.8 / 8.9	$-20.2 \pm 21.6 / -14.2 \pm 13.6$	17.1/24.4
4.13	4	$-4.8 \pm 5.2 / -5.1 \pm 4.9$	4.4 / 8.5	- / -	21.5/20.3	8.0/8.1	12.8 / 9.0	$-21.9 \pm 23.7 / -15.9 \pm 15.3$	20.1/26.5
4.13	5	$-5.2 \pm 5.8 / -5.8 \pm 5.6$	5.0 / 9.5	- / -	21.7/20.1	8.0/8.1	15.9 / 9.2	$-23.5 \pm 26.2 / -18.3 \pm 17.6$	22.6/29.9
4.14	0	$3.7 \pm 2.9 / 4.3 \pm 4.0$	9.7 / 12.0	1.6/1.2	22.5/20.9	8.0/8.1	7.6 / 8.6	$16.1 \pm 12.6 / 13.0 \pm 12.1$	42.3/36.3
4.14	1	$3.7 \pm 3.0 / 4.9 \pm 4.5$	9.9 / 13.4	1.5/1.2	22.1/20.8	8.0/8.1	7.9 / 9.7	$16.4 \pm 13.3 / 14.9 \pm 13.7$	43.9/40.8
4.14	2	$3.7 \pm 3.2 / 5.6 \pm 5.1$	10.5 / 15.2	1.3/1.2	21.9/20.5	8.0/8.1	9.8 / 12.2	$16.6 \pm 14.3 / 17.3 \pm 15.7$	47.0/46.9
4.14	3	$3.6 \pm 3.5 / 6.4 \pm 5.6$	11.0 / 17.0	1.2/1.3	21.7/20.1	8.0/8.1	12.0 / 13.5	$16.3 \pm 15.8 / 20.2 \pm 17.6$	49.7/53.5
4.14	4	$3.5 \pm 3.7 / 7.2 \pm 6.3$	11.5 / 19.0	1.0/1.3	21.5/20.2	8.0/8.1	14.7 / 14.7	$16.0 \pm 16.9 / 22.6 \pm 19.7$	52.4/59.5
4.14	5	$3.1 \pm 4.0 / 7.8 \pm 6.7$	12.0 / 20.5	0.8/1.3	21.6/20.1	8.0/8.1	15.8 / 15.8	$14.1 \pm 18.2 / 24.6 \pm 21.1$	54.5/64.6
4.15	0	$0.0 \pm 2.1 / 2.2 \pm 3.6$	5.4 / 9.7	- / 0.6	22.5/20.9	8.0/8.1	3.7 / 13.2	$0.0 \pm 9.2 / 6.7 \pm 10.9$	23.5/29.4
4.15	1	$-0.2 \pm 2.3 / 3.2 \pm 4.5$	5.6 / 12.0	- / 0.8	22.2/20.7	8.0/8.1	3.8 / 14.8	$-0.9 \pm 10.2 / 9.8 \pm 13.8$	24.7/36.7
4.15	2	$-0.3 \pm 2.6 / 4.7 \pm 5.2$	6.1 / 14.7	- / 1.0	21.8/20.5	8.0/8.1	5.2 / 13.3	$-1.3 \pm 11.7 / 14.5 \pm 16.1$	27.4/45.4
4.15	3	$-0.5 \pm 2.8 / 5.9 \pm 5.9$	6.7 / 16.8	- / 1.1	21.7/20.2	8.0/8.1	6.8 / 11.3	$-2.3 \pm 12.7 / 18.5 \pm 18.5$	30.3/52.6
4.15	4	$-0.7 \pm 3.1 / 7.5 \pm 6.4$	7.3 / 19.4	- / 1.3	21.5/20.2	8.0/8.1	9.0 / 9.3	$-3.2 \pm 14.1 / 23.5 \pm 20.1$	33.3/60.8
4.15	5	$-1.0 \pm 3.5 / 8.8 \pm 7.0$	7.9 / 21.8	- / 1.4	21.4/20.1	8.0/8.1	9.7 / 9.9	$-4.6 \pm 16.0 / 27.7 \pm 22.0$	36.2/68.6
4.16	0	$1.0 \pm 2.1 / -1.9 \pm 3.4$	5.7 / 6.7	0.5/ -	22.5/20.9	8.0/8.1	3.9 / 6.3	$4.4 \pm 9.2 / -5.8 \pm 10.3$	24.8/20.3
4.16	1	$0.9 \pm 2.3 / -1.6 \pm 3.8$	6.0 / 7.5	0.4/ -	22.2/20.7	8.0/8.1	5.2 / 5.6	$4.0 \pm 10.2 / -4.9 \pm 11.6$	26.5/22.9
4.16	2	$0.7 \pm 2.7 / -1.6 \pm 4.3$	6.6 / 8.3	0.3/ -	21.8/20.5	8.0/8.1	5.3 / 5.1	$3.1 \pm 12.1 / -4.9 \pm 13.3$	29.7/25.6
4.16	3	$0.6 \pm 3.0 / -1.5 \pm 4.8$	7.1 / 9.4	0.2/ -	21.6/20.2	8.0/8.1	6.2 / 5.6	$2.7 \pm 13.6 / -4.7 \pm 15.0$	32.2/29.5
4.16	4	$0.6 \pm 3.2 / -1.7 \pm 5.3$	7.5 / 10.2	0.2/ -	21.5/20.2	8.0/8.1	2.3 / 6.2	$2.7 \pm 14.6 / -5.3 \pm 16.6$	34.2/32.0
4.16	5	$0.5 \pm 3.5 / -1.7 \pm 5.7$	8.0 / 11.0	0.1/ -	21.3/20.0	8.0/8.1	3.1 / 5.8	$2.3 \pm 16.1 / -5.4 \pm 18.0$	36.8/34.8
4.17	0	$-2.9 \pm 2.0 / -2.1 \pm 2.8$	4.1 / 5.6	- / -	22.5/20.8	8.0/8.1	5.8 / 7.3	$-12.6 \pm 8.7 / -6.4 \pm 8.5$	17.9/17.0
4.17	1	$-2.4 \pm 2.2 / -2.6 \pm 3.2$	4.7 / 6.1	- / -	22.2/20.6	8.0/8.1	6.2 / 7.8	$-10.6 \pm 9.7 / -8.0 \pm 9.8$	20.8/18.7
4.17	2	$-2.5 \pm 2.5 / -3.2 \pm 3.7$	5.1 / 6.8	- / -	21.7/20.5	8.0/8.1	6.4 / 9.1	$-11.3 \pm 11.3 / -9.9 \pm 11.4$	23.0/21.0
4.17	3	$-2.3 \pm 2.8 / -3.9 \pm 4.4$	5.6 / 7.6	- / -	21.5/20.3	8.0/8.1	6.7 / 12.4	$-10.5 \pm 12.8 / -12.2 \pm 13.7$	25.5/23.7
4.17	4	$-2.4 \pm 3.1 / -4.4 \pm 4.8$	6.1 / 8.2	- / -	21.5/20.2	8.0/8.1	7.0 / 13.3	$-10.9 \pm 14.1 / -13.8 \pm 15.0$	27.8/25.7
4.17	5	$-2.6 \pm 3.3 / -5.0 \pm 5.4$	6.5 / 8.9	- / -	21.2/20.0	8.0/8.1	6.8 / 14.5	$-12.0 \pm 15.3 / -15.8 \pm 17.1$	30.1/28.2

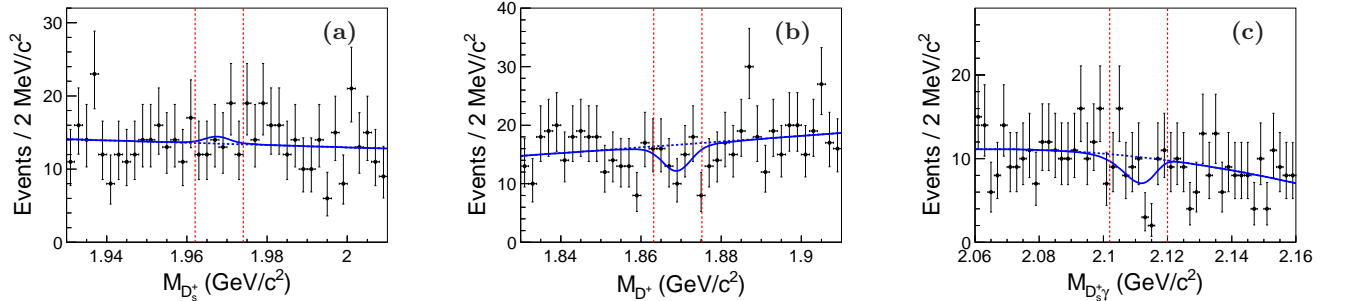


FIG. 6: The invariant-mass spectra of the (a) D_s^+ , (b) D^+ , and (c) D_s^{*+} candidates summed over four reconstructed modes from $\sqrt{s} = 10.520$ GeV data. The points with error bars represent the data, the solid curves show the results of the best fits to the data, and the blue dashed curves are the fitted backgrounds. The red dashed lines show the required signal regions.

listed in Table II.

Since the statistical significance in each case is less than 3σ , Bayesian upper limits at the 90% C.L. on N^{UL} are obtained using the same method as described in Sec. IV. The results for N^{UL} and product values of Born cross section and branching fraction ($\sigma^{\text{UL}}(e^+e^- \rightarrow R^{++} + \text{anything}) \times \mathcal{B}(R^{++} \rightarrow D^+ D_s^{*+})$) in e^+e^- collisions at

$\sqrt{s} = 10.520, 10.580$, and 10.867 GeV under typical assumptions of R^{++} mass with $\Gamma_{R^{++}}$ fixed at values ranging from 0 to 5 MeV are listed in Table II. The 90% C.L. upper limits on the product values of the $e^+e^- \rightarrow R^{++} + \text{anything}$ cross sections and the branching fraction of $R^{++} \rightarrow D^+ D_s^{*+}$ at $\sqrt{s} = 10.520, 10.580$, and 10.867 GeV for all hypothetical R^{++} masses with widths varying from 0 to 5 MeV are shown in Figs. 11(a)–(c),

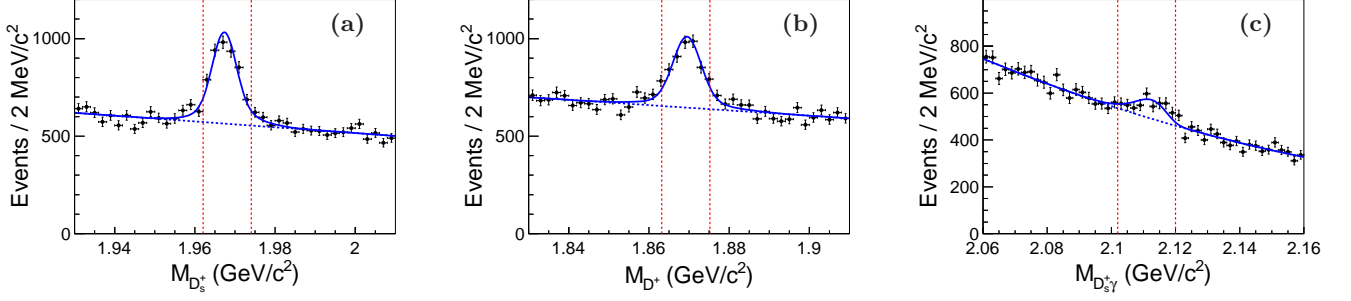


FIG. 7: The invariant-mass spectra of the (a) D_s^+ , (b) D^+ , and (c) D_s^{*+} candidates summed over four reconstructed modes from $\sqrt{s} = 10.580$ GeV data. The points with error bars represent the data, the solid curves show the results of the best fits to the data, and the blue dashed curves are the fitted backgrounds. The red dashed lines show the required signal regions.

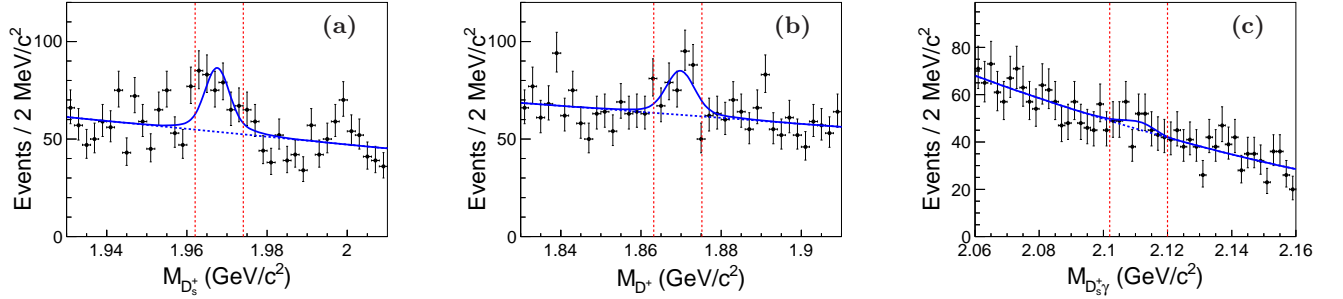


FIG. 8: The invariant-mass spectra of the (a) D_s^+ , (b) D^+ , and (c) D_s^{*+} candidates summed over four reconstructed modes from $\sqrt{s} = 10.867$ GeV data. The points with error bars represent the data, the solid curves show the results of the best fits to the data, and the blue dashed curves are the fitted backgrounds. The red dashed lines show the required signal regions.

respectively.

VI. SYSTEMATIC UNCERTAINTIES

The systematic uncertainties in the branching fraction and Born cross section measurements can be divided into two categories: multiplicative systematic uncertainties and additive systematic uncertainties.

The sources of multiplicative systematic uncertainties include detection-efficiency-related uncertainties, the statistical uncertainty of the MC efficiency, the modeling of MC event generation, branching fractions of intermediate states, energy dependence of the cross sections, the total numbers of $\Upsilon(1S, 2S)$ events as well as the integrated luminosity.

The detection-efficiency-related uncertainties include those for tracking efficiency (0.35% per track), particle identification efficiency (1.8% per kaon, 1.0% per pion), as well as momentum-weighted K_S^0 selection efficiency (2.2%) [55]. The photon reconstruction contributes 2.0% per photon, as determined from radiative Bhabha events. The above individual uncertainties from different reconstructed modes are added linearly, weighted by the

product of the detection efficiency and the product of all secondary branching fractions ($\epsilon_i \times \mathcal{B}_i$). Assuming these uncertainties are independent and adding them in quadrature, the final uncertainty related to the reconstruction efficiency is 6.6%.

The MC statistical uncertainties are estimated using the yields of selected and generated events; these are 1.0% or less. We use the EVTGEN generator to generate the signal MC samples. By changing the recoil mass of the R^{++} , the efficiencies are changed by (1–3)%. To be conservative, we take 1% and 3% as the systematical uncertainties related to signal MC statistics and generation.

The relative uncertainties of branching fractions for $D^+ \rightarrow K^-\pi^+\pi^+$, $D^+ \rightarrow K_S^0\pi^+$, $K_S^0 \rightarrow \pi^+\pi^-$, $D_s^{*+} \rightarrow \gamma D_s^+$, $D_s^+ \rightarrow \phi(\rightarrow K^+K^-)\pi^+$, and $D_s^+ \rightarrow \bar{K}^*(892)^0(\rightarrow K^-\pi^+)K^+$ are taken from Ref. [50] and summed in quadrature to obtain the total uncertainty of the branching fractions of the intermediate states for each reconstructed mode. The above individual uncertainties from different reconstructed modes are added linearly with a weighting factor of $\epsilon_i \times \mathcal{B}_i$ to obtain 2.5% as the uncertainty due to the branching fractions of intermediate states.

TABLE II: Summary of the 90% C.L. upper limits on the product values of Born cross sections and the branching fractions for $e^+e^- \rightarrow R^{++} + \text{anything}$ at $\sqrt{s} = 10.520, 10.580$, and 10.867 GeV with $R^{++} \rightarrow D^+ D_s^{*+}$ under typical assumptions of R^{++} mass ($M_{R^{++}}$ in GeV/ c^2) and width ($\Gamma_{R^{++}}$ in MeV) as examples, where N^{fit} is the number of fitted signal events, N^{UL} is the 90% C.L. upper limit on the number of signal events taking into account systematic uncertainties, $\Sigma(\sigma)$ is the local R^{++} significance, $\Sigma_i(\epsilon_i \mathcal{B}_i)$ is the sum of product of the detection efficiency and the product of all secondary branching fractions for each reconstruction mode, σ_{multi} is the total multiplicative systematic uncertainty, σ_{add} is the additive systematic uncertainty, $\sigma \times \mathcal{B}(\sigma(e^+e^- \rightarrow R^{++} + \text{anything}) \times \mathcal{B}(R^{++} \rightarrow D^+ D_s^{*+}))$ is the product value of Born cross section and branching fraction, and $\sigma^{\text{UL}} \times \mathcal{B}(\sigma^{\text{UL}}(e^+e^- \rightarrow R^{++} + \text{anything}) \times \mathcal{B}(R^{++} \rightarrow D^+ D_s^{*+}))$ is the 90% C.L. upper limit on the product value of Born cross section and branching fraction with systematic uncertainties included.

$e^+e^- \rightarrow R^{++} + \text{anything}$ at $\sqrt{s} = 10.520/10.580/10.867$ GeV, $R^{++} \rightarrow D^+ D_s^{*+}$														
$M_{R^{++}}$	$\Gamma_{R^{++}}$	N^{fit}		N^{UL}	$\Sigma(\sigma)$	$\Sigma_i(\epsilon_i \mathcal{B}_i) (\times 10^{-5})$	$\sigma_{\text{multi}}(\%)$	$\sigma_{\text{add}}(\%)$	$\sigma \times \mathcal{B}$ (fb)			$\sigma^{\text{UL}} \times \mathcal{B}$ (fb)		
4.13	0	1.4 \pm 2.3	/-24.6 \pm 17.8/	0.4 \pm 5.2	6.6 / 22.6 / 11.2	0.7/ - / 0.1	22.4/18.9/20.4	7.9	6.7 / 8.7 / 6.7	91.6 \pm 150.4	/-239.8 \pm 173.5/	21.2 \pm 275.9	431.7/	220.3 / 594.2
4.13	1	1.3 \pm 2.5	/-25.5 \pm 19.9/	0.4 \pm 5.9	7.1 / 25.6 / 12.4	0.5/ - / 0.1	22.2/18.8/19.7	7.9	8.3 / 9.2 / 6.3	85.8 \pm 165.0	/-249.9 \pm 195.0/	22.0 \pm 324.2	468.6/	250.9 / 681.3
4.13	2	1.0 \pm 2.9	/-27.0 \pm 22.9/	0.1 \pm 6.7	7.8 / 30.1 / 14.2	0.4/ - / 0.1	22.1/18.7/19.9	7.9	11.8/ 9.9 / 6.5	66.3 \pm 192.3	/-266.0 \pm 225.6/	5.4 \pm 364.4	517.1/	296.5 / 772.3
4.13	3	0.8 \pm 3.1	/-27.7 \pm 26.8/	-0.2 \pm 7.7	8.3 / 36.6 / 15.6	0.3/ - / -	21.8/18.5/20.0	7.9	12.9/11.2/ 6.9	53.8 \pm 208.3	/-275.8 \pm 266.9/	-10.8 \pm 416.7	557.8/	364.5 / 844.3
4.13	4	0.7 \pm 3.4	/-27.5 \pm 30.0/	-0.5 \pm 8.5	8.9 / 42.6 / 17.1	0.2/ - / -	21.5/18.7/19.4	7.9	14.2/13.5/ 7.3	47.7 \pm 231.7	/-270.9 \pm 295.6/	-27.9 \pm 474.2	606.5/	419.7 / 954.1
4.13	5	0.3 \pm 3.7	/-27.5 \pm 32.8/	-0.7 \pm 9.5	9.4 / 47.8 / 18.8	0.1/ - / -	21.4/18.5/19.1	7.9	15.7/13.8/ 7.9	20.5 \pm 253.3	/-273.9 \pm 326.6/	-39.7 \pm 538.4	643.6/	476.0 / 1065.4
4.14	0	-3.5 \pm 1.2/	30.8 \pm 18.3 /	-4.7 \pm 4.1	3.1 / 58.6 / 6.5	- / 1.7/ -	22.4/18.8/20.3	7.9	10.5/ 8.7 / 15.9	-228.9 \pm 78.5 /	301.8 \pm 179.3 /	-250.6 \pm 218.6	202.8/	574.2 / 346.6
4.14	1	-4.0 \pm 1.3/	37.4 \pm 21.4 /	-7.1 \pm 4.8	3.3 / 68.8 / 7.1	- / 1.8/ -	22.2/18.7/19.8	7.9	11.8/ 6.8 / 10.2	-264.0 \pm 85.8 /	368.5 \pm 210.8 /	-388.1 \pm 262.4	217.8/	677.8 / 388.1
4.14	2	-4.6 \pm 1.5/	43.3 \pm 24.2 /	-8.9 \pm 7.0	3.6 / 78.1 / 7.9	- / 1.8/ -	22.0/18.7/19.9	7.9	12.2/ 7.6 / 8.9	-306.3 \pm 99.9 /	426.6 \pm 238.4 /	-484.1 \pm 380.7	239.7/	769.4 / 429.7
4.14	3	-5.2 \pm 1.7/	49.0 \pm 27.2 /	-10.9 \pm 6.5	4.0 / 87.4 / 8.8	- / 1.8/ -	21.8/18.4/19.9	7.9	13.5/ 9.2 / 7.9	-349.5 \pm 114.3/	490.6 \pm 272.3 /	-592.9 \pm 353.5	268.8/	875.1 / 478.6
4.14	4	-6.1 \pm 1.9/	54.6 \pm 30.4 /	-12.5 \pm 7.4	4.4 / 97.2 / 9.7	- / 1.8/ -	21.5/18.5/19.4	7.9	12.9/10.5/ 6.5	-415.7 \pm 129.5/	543.7 \pm 302.7 /	-697.4 \pm 412.9	299.8/	967.9 / 541.2
4.14	5	-6.6 \pm 2.2/	58.7 \pm 32.9 /	-13.2 \pm 7.9	4.8 / 104.7/10.9	- / 1.8/ -	21.4/18.3/19.2	7.9	13.2/11.8/ 6.1	-451.9 \pm 150.6/	590.9 \pm 331.2 /	-744.1 \pm 445.4	328.6/	1054.0/ 614.5
4.15	0	0.2 \pm 2.3 /	2.2 \pm 17.5 /	-0.9 \pm 5.3	6.3 / 37.0 / 10.4	0.1/0.1/ -	22.4/18.8/20.3	7.9	6.7 / 10.0/ 7.4	13.1 \pm 150.4 /	21.6 \pm 171.5 /	-48.0 \pm 282.6	412.1/	362.6 / 554.5
4.15	1	0.4 \pm 2.6 /	1.8 \pm 19.9 /	-0.4 \pm 6.0	6.8 / 41.7 / 11.7	0.1/0.1/ -	22.3/18.6/19.8	7.9	7.5 / 11.4/ 6.8	26.3 \pm 170.8 /	17.8 \pm 197.1 /	-21.9 \pm 328.0	446.8/	413.0 / 639.6
4.15	2	0.5 \pm 2.9 /	4.3 \pm 23.3 /	0.1 \pm 6.9	7.6 / 51.1 / 13.3	0.2/0.1/0.1	21.9/18.6/19.9	7.9	9.3 / 12.3/ 5.3	33.4 \pm 194.0 /	42.6 \pm 230.8 /	5.4 \pm 375.3	508.4/	506.1 / 723.4
4.15	3	0.6 \pm 3.3 /	7.0 \pm 26.3 /	0.7 \pm 7.8	8.4 / 59.0 / 15.2	0.2/0.1/0.1	21.8/18.4/19.8	7.9	11.9/13.5/ 5.1	40.3 \pm 221.8 /	70.1 \pm 263.3 /	38.3 \pm 426.4	564.5/	590.7 / 830.9
4.15	4	0.6 \pm 3.5 /	11.3 \pm 29.4 /	0.9 \pm 8.5	9.1 / 67.8 / 16.5	0.2/0.5/0.1	21.5/18.4/19.5	7.9	13.4/13.8/ 4.8	40.9 \pm 238.5 /	113.8 \pm 294.4 /	50.0 \pm 471.8	620.1/	678.8 / 915.9
4.15	5	0.7 \pm 3.9 /	15.4 \pm 32.0 /	1.7 \pm 9.4	9.9 / 74.0 / 18.5	0.2/0.5/0.2	21.4/18.1/19.3	7.9	15.3/14.7/ 5.2	47.9 \pm 267.0 /	156.7 \pm 325.7 /	95.3 \pm 527.2	677.8/	753.2 / 1037.5
4.16	0	0.4 \pm 2.6 /	9.1 \pm 17.9 /	2.5 \pm 5.5	7.2 / 40.1 / 12.4	0.2/0.5/0.5	22.4/18.7/20.2	7.9	10.2/14.8/11.6	26.2 \pm 170.1 /	89.7 \pm 176.3 /	134.0 \pm 294.7	470.9/	395.1 / 664.4
4.16	1	1.1 \pm 3.1 /	10.3 \pm 20.3 /	4.3 \pm 6.4	8.4 / 45.6 / 15.1	0.4/0.5/0.7	22.3/18.5/19.9	7.9	9.7 / 13.7/10.5	72.3 \pm 203.7 /	102.6 \pm 202.2 /	233.9 \pm 348.1	551.9/	454.1 / 821.3
4.16	2	1.9 \pm 3.5 /	12.7 \pm 23.9 /	6.2 \pm 7.5	9.7 / 53.8 / 18.0	0.6/0.5/0.9	21.8/18.6/19.9	7.9	11.4/14.5/ 9.7	127.7 \pm 235.2 /	125.8 \pm 236.7 /	337.2 \pm 407.9	651.9/	532.9 / 979.0
4.16	3	2.7 \pm 3.9 /	14.3 \pm 26.8 /	9.1 \pm 8.6	11.0/ 59.8 / 21.8	0.7/0.5/1.1	21.8/18.3/19.8	7.9	12.5/15.3/10.4	181.5 \pm 262.1 /	144.0 \pm 269.8 /	497.5 \pm 470.1	739.3/	602.0 / 1191.7
4.16	4	3.3 \pm 4.3 /	14.3 \pm 29.0 /	11.5 \pm 9.6	12.2/ 64.2 / 25.1	0.8/0.5/1.3	21.4/18.2/19.5	7.9	13.2/15.9/12.3	225.9 \pm 294.4 /	144.8 \pm 293.5 /	638.3 \pm 532.9	835.2/	649.9 / 1393.2
4.16	5	3.5 \pm 4.5 /	18.1 \pm 32.5 /	13.1 \pm 10.3	12.8/ 73.5 / 28.5	0.8/0.6/1.3	21.3/17.9/19.4	7.9	13.1/16.3/13.2	240.7 \pm 209.5 /	186.3 \pm 334.5 /	730.9 \pm 574.7	880.4/	756.5 / 1590.1
4.17	0	-2.2 \pm 1.3/-	16.0 \pm 17.2/	1.7 \pm 5.3	3.4 / 22.1 / 11.3	- / - / 0.3	22.4/18.6/20.1	7.9	8.5 / 11.9/10.8	-143.9 \pm 85.0 /	-158.5 \pm 170.4/	91.5 \pm 285.4	222.4/	218.9 / 608.5
4.17	1	-2.7 \pm 1.5/-	20.9 \pm 20.0/	1.4 \pm 5.9	3.8 / 24.5 / 12.1	- / - / 0.2	22.4/18.4/20.0	7.9	6.7 / 10.8/12.7	-176.6 \pm 98.1 /	-209.3 \pm 200.2/	75.8 \pm 319.3	248.5/	245.3 / 654.8
4.17	2	-3.3 \pm 1.8/-	27.1 \pm 22.9/	1.3 \pm 6.7	4.3 / 26.8 / 13.5	- / - / 0.2	21.7/18.6/19.9	7.9	5.8 / 12.4/13.5	-222.8 \pm 121.5/-	-268.4 \pm 226.8/	70.7 \pm 364.4	290.3/	265.4 / 734.3
4.17	3	-3.8 \pm 2.1/-	33.1 \pm 25.9/	1.1 \pm 7.5	4.7 / 29.1 / 14.8	- / - / 0.1	21.7/18.2/19.7	7.9	4.1 / 13.2/14.9	-256.6 \pm 141.8/-	-335.1 \pm 262.2/	60.4 \pm 412.1	317.3/	294.6 / 813.2
4.17	4	-4.2 \pm 2.5/-	37.3 \pm 28.3/	1.0 \pm 8.5	5.1 / 31.1 / 16.2	- / - / 0.1	21.4/18.0/19.5	7.9	3.3 / 13.9/16.1	-287.5 \pm 171.2/-	-381.8 \pm 289.6/	55.5 \pm 471.8	349.2/	318.3 / 899.2
4.17	5	-4.6 \pm 2.8/-	43.5 \pm 31.6/	1.1 \pm 9.3	5.5 / 33.8 / 17.8	- / - / 0.1	21.3/17.7/19.5	7.9	2.3 / 15.8/16.4	-316.4 \pm 192.6/-	-452.8 \pm 328.9/	61.1 \pm 516.2	378.3/	351.8 / 988.0

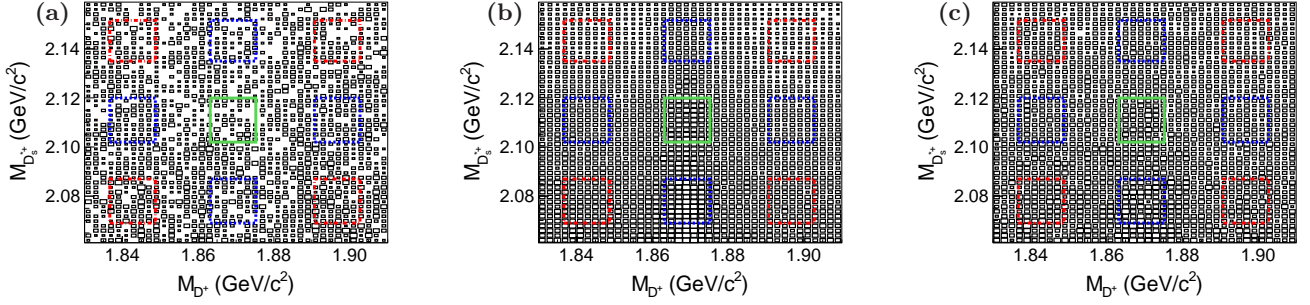


FIG. 9: The scatter plots of $M_{D_s^{*+}}$ versus $M_{D^{*+}}$ from (a) $\sqrt{s} = 10.520$ GeV, (b) $\sqrt{s} = 10.580$ GeV, and (c) $\sqrt{s} = 10.867$ GeV data samples. The central solid boxes define the signal regions, and the red dash-dotted and blue dashed boxes show the $M_{D^{*+}}$ and $M_{D_s^{*+}}$ sideband regions described in the text.

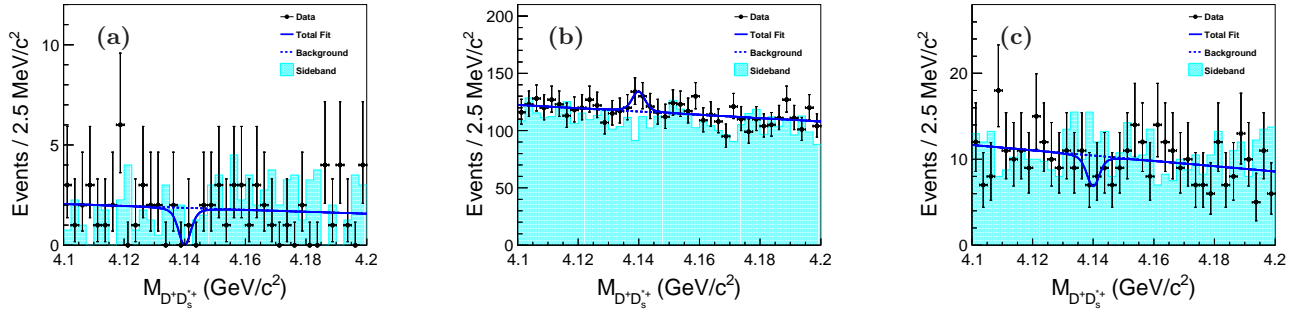


FIG. 10: The invariant-mass spectra of the $D^+ D_s^{*+}$ from $e^+ e^-$ annihilations at (a) $\sqrt{s} = 10.520$ GeV, (b) $\sqrt{s} = 10.580$ GeV, and (c) $\sqrt{s} = 10.867$ GeV data samples. The cyan shaded histograms are from the normalized $M_{D^{*+}}$ and $M_{D_s^{*+}}$ sideband events. The blue solid curves show the fitted results with the R^{++} mass fixed at $4.14 \text{ GeV}/c^2$ and width fixed at 2 MeV , and the blue dashed curves are the fitted backgrounds.

Changing the s dependence of the cross sections of $e^+ e^- \rightarrow R^{++} + \text{anything}$ from $1/s$ to $1/s^4$, the radiative correction factors $(1 + \delta)_{\text{ISR}}$ become 0.712, 0.711, and 0.709 for $\sqrt{s} = 10.520$, 10.580, and 10.867 GeV, respectively. The differences are less than 0.3%. Thus, the systematic uncertainty related to the radiative correction factors is negligible with respect to the other sources.

The uncertainties on the total numbers of $\Upsilon(1S)$ and $\Upsilon(2S)$ events are 2.0% and 2.3%, respectively, which are mainly due to imperfect simulations of the charged track multiplicity distributions from inclusive hadronic MC events. The total luminosity is determined to 1.4% precision using wide-angle Bhabha scattering events.

Additive systematic uncertainties due to the mass resolution and fit are considered as follows. The uncertainty due to the mass resolution is studied by using the control sample of $B^0 \rightarrow D^- D_s^{*+}$; the difference in mass resolution between MC simulation and data is around 10%. Thus, the uncertainty due to the mass resolution is estimated by enlarging the mass resolution by 10% when fitting the $D^+ D_s^{*+}$ invariant-mass distributions. To estimate the uncertainties

associated with the fit, the order of the background polynomial is changed from first to second or third and the range of the fit is changed by $\pm 30 \text{ MeV}/c^2$.

The upper limits on the branching fraction and Born cross section at the 90% C.L. are determined and the systematic uncertainties are taken into account in two steps. First, when we study the additive systematic uncertainties described above, we take the most conservative upper limit at the 90% C.L. on the number of R^{++} signal yields. The differences between the most conservative upper limits and the nominal fits are in the range of 2.3% – 16.4% (see Tables I and II for detailed values), depending on the center-of-mass energy, the mass and width of the R^{++} state. Then, to take into account the multiplicative systematic uncertainties, the likelihood with the most conservative upper limit is convolved with a Gaussian function whose width is the corresponding total multiplicative systematic uncertainty.

The sources of uncertainties are assumed independent, and the total multiplicative systematic uncertainties are obtained by adding all uncertainties in quadrature. The total multiplicative systematic uncertainties are listed in

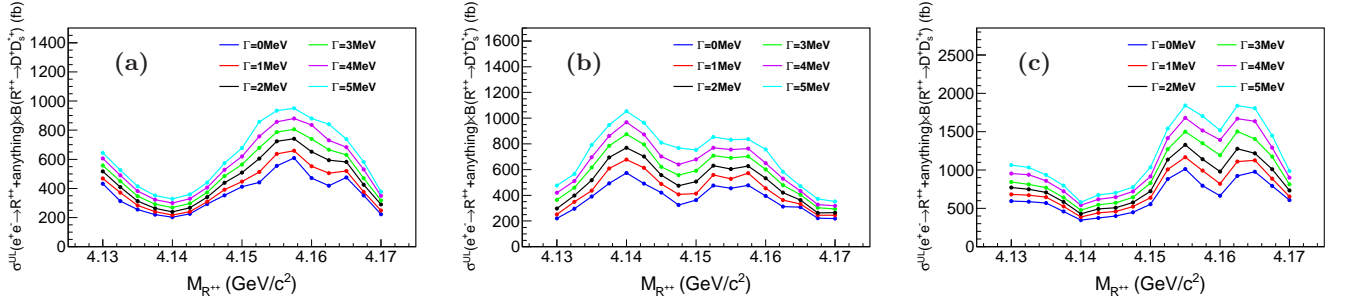


FIG. 11: The 90% C.L. upper limits on the product values of the $e^+e^- \rightarrow R^{++} + \text{anything}$ cross sections and the branching fraction of $R^{++} \rightarrow D^+ D_s^{*+}$ at (a) $\sqrt{s} = 10.520$ GeV, (b) $\sqrt{s} = 10.580$ GeV, and (c) $\sqrt{s} = 10.867$ GeV as a function of the assumed R^{++} masses with widths varying from 0 to 5 MeV in steps of 1 MeV.

Tables I and II for the measurements of $\mathcal{B}(\Upsilon(1S, 2S) \rightarrow R^{++} + \text{anything}) \times \mathcal{B}(R^{++} \rightarrow D^+ D_s^{*+})$ and $\sigma(e^+e^- \rightarrow R^{++} + \text{anything}) \times \mathcal{B}(R^{++} \rightarrow D^+ D_s^{*+})$ at $\sqrt{s} = 10.520$, 10.580, and 10.867 GeV, respectively.

VII. CONCLUSION

In summary, using the data samples of 102 million $\Upsilon(1S)$ events, and 158 million $\Upsilon(2S)$ events, as well as 89.45 fb^{-1} , 711 fb^{-1} , and 121.06 fb^{-1} collected at $\sqrt{s} = 10.520$, 10.580, and 10.867 GeV, we search for the doubly-charged DDK bound state decaying to $D^+ D_s^{*+}$, referred to as R^{++} , both in $\Upsilon(1S, 2S)$ inclusive decays and in e^+e^- annihilations. No evident signals are observed in all studied reactions. We determine the 90% C.L. upper limits on $\mathcal{B}(\Upsilon(1S, 2S) \rightarrow R^{++} + \text{anything}) \times \mathcal{B}(R^{++} \rightarrow D^+ D_s^{*+})$ and $\sigma(e^+e^- \rightarrow R^{++} + \text{anything}) \times \mathcal{B}(R^{++} \rightarrow D^+ D_s^{*+})$ at $\sqrt{s} = 10.520$, 10.580, and 10.867 GeV under different assumptions of R^{++} masses varying from 4.13 to 4.17 GeV/c^2 in steps of 2.5 MeV/c^2 and widths varying from 0 to 5 MeV in steps of 1 MeV.

VIII. ACKNOWLEDGMENTS

We thank Professor Li-sheng Geng for useful discussions and comments. We thank the KEKB group for the excellent operation of the accelerator; the KEK cryogenics group for the efficient operation of the solenoid; and the KEK computer group, and the Pacific Northwest National Laboratory (PNNL) Environmental Molecular Sciences Laboratory (EMSL) computing group for strong computing support; and the National Institute of Informatics, and Science Information NETwork 5 (SINET5) for valuable network support. We acknowledge support from the Ministry of Education, Culture, Sports, Science, and Technology (MEXT) of Japan, the Japan

Society for the Promotion of Science (JSPS), and the Tau-Lepton Physics Research Center of Nagoya University; the Australian Research Council including grants DP180102629, DP170102389, DP170102204, DP150103061, FT130100303; Austrian Science Fund (FWF); the National Natural Science Foundation of China under Contracts No. 11435013, No. 11475187, No. 11521505, No. 11575017, No. 11675166, No. 11705209, No. 11761141009, No. 11975076, No. 12005040; Key Research Program of Frontier Sciences, Chinese Academy of Sciences (CAS), Grant No. QYZDJ-SSW-SLH011; the CAS Center for Excellence in Particle Physics (CCEPP); the Shanghai Pujiang Program under Grant No. 18PJ1401000; the Ministry of Education, Youth and Sports of the Czech Republic under Contract No. LTT17020; the Carl Zeiss Foundation, the Deutsche Forschungsgemeinschaft, the Excellence Cluster Universe, and the VolkswagenStiftung; the Department of Science and Technology of India; the Istituto Nazionale di Fisica Nucleare of Italy; National Research Foundation (NRF) of Korea Grant Nos. 2016R1D1A1B01010135, 2016R1D1A1B02012900, 2018R1A2B3003643, 2018R1A6A1A06024970, 2018R1D1A1B07047294, 2019K1A3A7A09033840, 2019R1I1A3A01058933; Radiation Science Research Institute, Foreign Large-size Research Facility Application Supporting project, the Global Science Experimental Data Hub Center of the Korea Institute of Science and Technology Information and KREONET/GLORIAD; the Polish Ministry of Science and Higher Education and the National Science Center; Russian Science Foundation, Grant No. 18-12-00226; University of Tabuk research grants S-0256-1438 and S-0280-1439 (Saudi Arabia); the Slovenian Research Agency; Ikerbasque, Basque Foundation for Science, Spain; the Swiss National Science Foundation; the Ministry of Education and the Ministry of Science and Technology of Taiwan; and the United States Department of Energy and the National Science Foundation.

-
- [1] B. Aubert *et al.* (BABAR Collaboration), Phys. Rev. Lett. **90**, 242001 (2003).
 - [2] D. Besson *et al.* (CLEO Collaboration), Phys. Rev. D **68**, 032002 (2003).
 - [3] P. Krokovny *et al.* (Belle Collaboration), Phys. Rev. Lett. **91**, 262002 (2003).
 - [4] S. Godfrey and N. Isgur, Phys. Rev. D **32**, 189 (1985).
 - [5] S. Godfrey and R. Kokoski, Phys. Rev. D **43**, 1679 (1991).
 - [6] J. Zeng, J. W. Van Orden, and W. Roberts, Phys. Rev. D **52**, 5229 (1995).
 - [7] D. Ebert, V. O. Galkin, and R. N. Faustov, Phys. Rev. D **57**, 5663 (1998).
 - [8] Y. S. Kalashnikova, A. V. Nefediev, and Y. A. Simonov, Phys. Rev. D **64**, 014037 (2001).
 - [9] M. Di Pierro and E. Eichten, Phys. Rev. D **64**, 114004 (2001).
 - [10] G. S. Bali, Phys. Rev. D **68**, 071501 (2003).
 - [11] A. Dougall *et al.* (UKQCD Collaboration), Phys. Lett. B **569**, 41 (2003).
 - [12] T. Barnes, F. E. Close, and H. J. Lipkin, Phys. Rev. D **68**, 054006 (2003).
 - [13] E. E. Kolomeitsev and M. F. M. Lutz, Phys. Lett. B **582**, 39 (2004).
 - [14] F. K. Guo, P. N. Shen, H. C. Chiang, R. G. Ping, and B. S. Zou, Phys. Lett. B **641**, 278 (2006).
 - [15] D. Gamermann, E. Oset, D. Strottman, and M. J. Vicente Vacas, Phys. Rev. D **76**, 074016 (2007).
 - [16] F. K. Guo, C. Hanhart, and U. G. Meißner, Eur. Phys. J. A **40**, 171 (2009).
 - [17] M. Cleven, F. K. Guo, C. Hanhart, and U. G. Meißner, Eur. Phys. J. A **47**, 19 (2011).
 - [18] H. Y. Cheng and W. S. Hu, Phys. Lett. B **566**, 193 (2003).
 - [19] Y. Q. Chen and X. Q. Li, Phys. Rev. Lett. **93**, 232001 (2004).
 - [20] V. Dmitrasinovic, Phys. Rev. Lett. **94**, 162002 (2005).
 - [21] E. van Beveran and G. Rupp, Phys. Rev. Lett. **91**, 012003 (2003).
 - [22] K. Terasaki, Phys. Rev. D **68**, 011501 (2003).
 - [23] T. E. Browder, S. Pakvasa, and A. A. Petrov, Phys. Lett. B **578**, 365 (2004).
 - [24] L. Maiani, F. Piccinini, A. D. Polosa, and V. Riquer, Phys. Rev. D **71**, 014028 (2005).
 - [25] M. E. Bracco, A. Lozea, R. D. Matheus, F. S. Navarra, and M. Nielsen, Phys. Lett. B **624**, 217 (2005).
 - [26] L. Liu, K. Orginos, F. K. Guo, C. Hanhart, and U. G. Meißner, Phys. Rev. D **87**, 014508 (2013).
 - [27] D. Mohler *et al.*, Phys. Rev. Lett. **111**, 222001 (2013).
 - [28] C. B. Lang *et al.*, Phys. Rev. D **90**, 034510 (2014).
 - [29] M. Ablikim *et al.* (BESIII Collaboration), Phys. Rev. D **97**, 051103 (2017).
 - [30] S. Godfrey, Phys. Lett. B **568**, 254 (2003).
 - [31] A. Faessler, T. Gutsche, V. E. Lyubovitskij, and Y. L. Ma, Phys. Rev. D **76**, 014005 (2007).
 - [32] M. Cleven, H. W. Griebhammer, F. K. Guo, C. Hanhart, and U. G. Meißner, Eur. Phys. J. A **50**, 149 (2014).
 - [33] W. A. Bardeen, E. J. Eichten, and C. T. Hill, Phys. Rev. D **68**, 054024 (2003).
 - [34] M. A. Nowak, M. Rho, and I. Zahed, Acta Phys. Polon. B **35** (2004) 2377.
 - [35] M. S. Sanchez, L. S. Geng, J. X. Lu, T. Hyodo, and M. P. Valderrama, Phys. Rev. D **98**, 054001 (2018).
 - [36] A. M. Torres, K. Khemchandani, and L. S. Geng, Phys. Rev. D **99**, 076017 (2019).
 - [37] T. W. Wu, M. Z. Liu, L. S. Geng, E. Hiyama, and M. P. Valderrama, Phys. Rev. D **100**, 034029 (2019).
 - [38] Y. Huang, M. Z. Liu, Y. W. Pan, L. S. Geng, A. M. Torres, and K. P. Khemchandani, Phys. Rev. D **101**, 014022 (2020).
 - [39] R. Aaij *et al.* (LHCb Collaboration), Phys. Rev. Lett. **119**, 112001 (2017).
 - [40] M. Karliner and J. L. Rosner, Phys. Rev. Lett. **119**, 202001 (2017).
 - [41] E. J. Eichten and C. Quigg, Phys. Rev. Lett. **119**, 202002 (2017).
 - [42] A. Abashian *et al.* (Belle Collaboration), Nucl. Instrum. Methods Phys. Res., Sect. A **479**, 117 (2002); also, see detector section in J. Brodzicka *et al.*, Prog. Theor. Exp. Phys. **2012**, 04D001 (2012).
 - [43] S. Kurokawa and E. Kikutani, Nucl. Instrum. Methods Phys. Res., Sect. A **499**, 1 (2003), and other papers included in this volume; T. Abe *et al.*, Prog. Theor. Exp. Phys. **2013**, 03A001 (2013), and references therein.
 - [44] D. J. Lange, Nucl. Instrum. Methods Phys. Res., Sect. A **462**, 152 (2001).
 - [45] R. Brun *et al.*, GEANT 3: user's guide Geant 3.10, Geant 3.11, CERN Report No. DD/EE/84-1, 1984.
 - [46] E. Nakano, Nucl. Instrum. Methods Phys. Res., Sect. A **494**, 402 (2002).
 - [47] M. Feindt and U. Kerzel, Nucl. Instrum. Methods Phys. Res., Sect. A **559**, 190 (2006).
 - [48] H. Nakano, Ph.D. Thesis, Tohoku University (2014) Chapter 4, unpublished, https://tohoku.repo.nii.ac.jp/?action=pages_view_main&active_action=repository_view_main_item_detail&item_id=70563&item_no=1&page_id=33&block_id=38.
 - [49] G. Punzi, eConf **C030908**, MODT002 (2003). arXiv:physics/0308063.
 - [50] P. A. Zyla *et al.* (Particle Data Group), Prog. Theor. Exp. Phys. **2020**, 083C01 (2020).
 - [51] The Novosibirsk function is defined as $f(x) = \exp[-\frac{1}{2}(\ln^2(1 + \Lambda(x - x_0))/\tau^2 + \tau^2)]$ with $\Lambda = \sinh(\tau\sqrt{\ln 4})/(\sigma\sqrt{\ln 4})$. The parameters represent the mean (x_0), the width (σ) and the tail asymmetry (τ).
 - [52] X. Y. Zhou, S. X. Du, G. Li, and C. P. Shen, Comput. Phys. Commun. **258**, 107540 (2021).
 - [53] E. A. Kuraev and V. S. Fadin, Yad. Fiz. **41**, 733 (1985) [Sov. J. Nucl. Phys. **41**, 466 (1985)].
 - [54] S. Actis *et al.*, Eur. Phys. J. C **66**, 585 (2010).
 - [55] N. Dash *et al.* (Belle Collaboration), Phys. Rev. Lett. **119**, 171801 (2007).